Acumentrics Final Quarterly Report and Project Summary

Project Title:
Generation and Solid Oxide Fuel Cell Carbon Sequestration in Northwest Indiana

Project Period:
July 1st – September 30th

Date of Report:
September 30th, 2007

Recipient:
NiSource Energy Technologies, Inc.

Award Number:
DE-FC36-04GO14227

Working Partners:
Acumentrics Corporation

Cost-Sharing Partners:
Acumentrics Corporation

Contact:
Rich Sichtermann, 219-647-4441, rhsichtermann@nisource.com
Norm Bessette, 781-461-8251, nbessette@acumentrics.com

DOE Managers:
Reginald Tyler, 303-275-4929, Reginald.tyler@go.doe.gov

Project Objective:

The objective of the project is to develop the technology capable of capturing all carbon monoxide and carbon dioxide from a natural gas fueled Solid Oxide Fuel Cell (SOFC) system. In addition, the technology to electrochemically oxidize any remaining carbon monoxide to carbon dioxide will be developed. Success of this R&D program would allow for the generation of electrical power and thermal power from a fossil fuel driven SOFC system without the carbon emissions resulting from any other fossil fueled power generation system.

Background:

In a solid oxide fuel cell (SOFC) the exhaust consists of carbon dioxide and steam as well as unutilized hydrogen and carbon monoxide. Normally this gas stream is mixed with the air stream and combusted prior to release from the machine. At this point, the carbon dioxide is very dilute (<10 vol%) and is therefore impractical to capture. Due to this low concentration, most fuel cell systems as well as all combustion driven machinery have a difficulty in recovering carbon dioxide. Acumentrics' solid oxide fuel cell technology is unique in that it provides for the potential of completely separate pathways for spent fuel and air. This gives the Acumentrics SOFC the flexibility to either direct the exhaust back to the fuel input to provide steam for reforming hydrocarbon fuels or further oxidize the exhaust gas stream into carbon dioxide and water vapor. This water can then be condensed leaving a concentrated carbon dioxide stream that is now free of non-condensables or other gases.

In a typical solid oxide fuel cell, the following reactions occur:

First, the oxygen present in air is dissociated and reduced at the cathode.

$O_2 \rightarrow 2\ O + 4e\text{-} \rightarrow 2\ O^{2-}$

Next, the reformed hydrocarbon fuel is oxidized at the anode after the oxygen ions have passed across the yttria stabilized zirconia electrolyte.

$H_2 + 2\ O^{2-} \rightarrow H_2O + 4\ e\text{-}$

$CO + 2\ O^{2-} \rightarrow CO_2 + 4\ e\text{-}$

The electrons from the reaction are then released to an external circuit providing export power.

The problem that occurs is that the incoming hydrocarbon fuel is not 100% electrochemically oxidized into carbon dioxide and steam due to limitations on the anode material. If the existing SOFC technology were pushed to 100% fuel utilization, the present nickel based anode would have a tendency to oxidize to nickel oxide, which would increase its volume by nearly 55% thereby cracking the zirconia electrolyte and allowing the fuel and oxidant streams to communicate.

To avoid this problem, this development program will develop a solid-state ceramic device, similar to an SOFC, whereby oxygen would still be dissociated and reduced at a cathode layer and these oxygen ions would continue to pass across an electrolyte layer. The difference being that the fuel would then be oxidized at the anode/electrolyte interface and the electrons would pass back through the electrolyte rather than through an external circuit thereby making the electrolyte layer a mixed conductor (conducting electrons *and* ions) rather than a pure ionic conductor. In essence, the ceramic device would act as a fuel cell, which is continuously short-circuited and does not export power. To complete this concept, a material capable of transporting oxygen ions as well as electrons across it must be developed. This material must maintain its stability at temperature as well as handle the internal heat generated since all energy would be dissipated as heat on the material's surface as opposed to the fuel cell where approximately half of the energy is dissipated as heat while half is removed as work (electrical power).

Task 1: Conceptual design of a tubular SOFC low carbon emission generator:

In order to take full advantage of the fuel cell technology's ability to lower overall carbon emissions, the fuel cell module must be incorporated in to a system that can economically, reliably and efficiently meet the power needs of the individual user. For the residential user, integration of the fuel cell with the homes central heating and domestic hot water systems provide a means to produce affordable electric power while recovering the fuel cells thermal energy. In this Combined Heat and Power configuration the fuel cells thermal output is supplemented by a peak burner system during periods of high thermal demand. This arrangement is illustrated in the Process and Instrumentation Diagram (Figure 1).

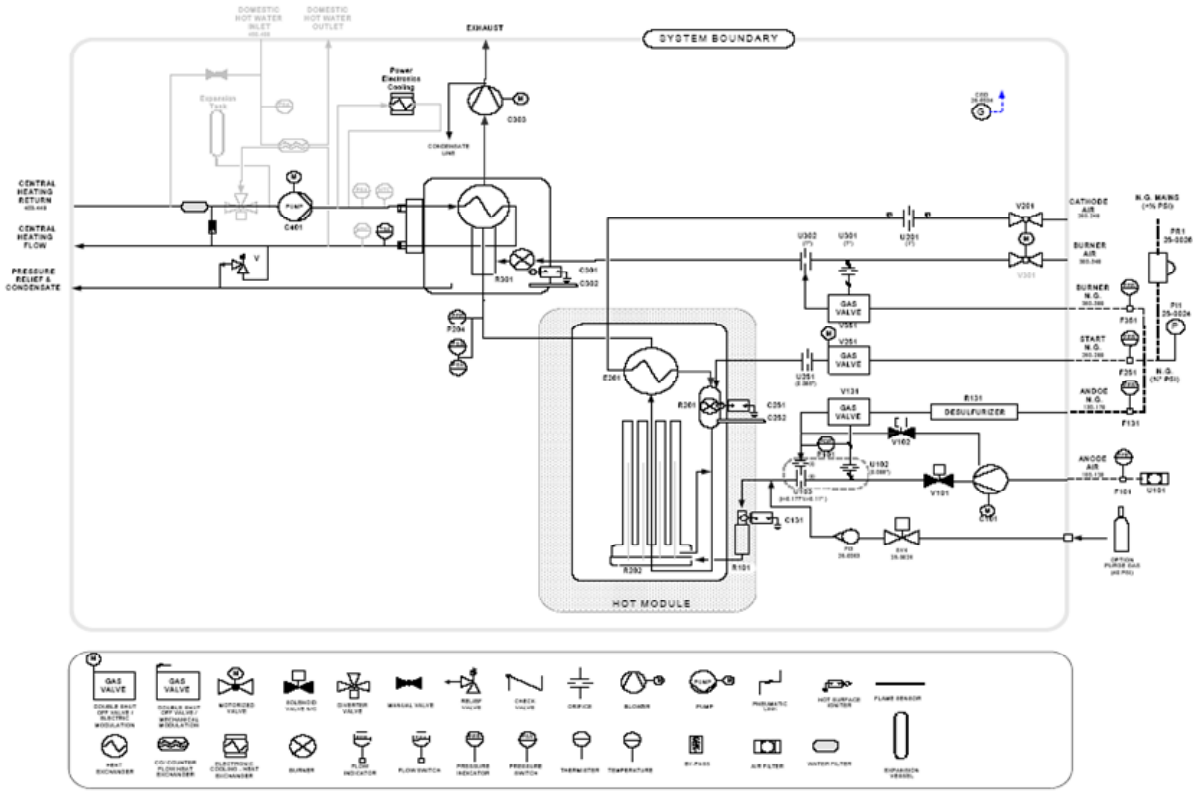

Figure 1 Combined Heat and Power P&ID

As shown (Figure 1), a common hot water coil is utilized to recover the fuel cell thermal output as well as that provided by the peak burner. In keeping with the requirement to minimize carbon emissions through high efficiency operation, a condensing coil is utilized which enables recovery of the fuels latent heat. To reduce system cost further a single induced draft blower is utilized to provide air for both the fuel cell and peak burner. On the fuel cell anode side the venturi metering system described in previous reports is utilized to reduce system component costs and to ensure that an anode stream with the correct oxygen to carbon ratio is delivered to the fuel cell under all operating conditions without the need for expensive flow meters. The flow meters shown outside the system boundary on the P&ID are included for full characterization of a prototype system.

Figure 2 & Figure 3 show the actual system configuration. The CHP unit has been configured so that it can be either a floor standing or wall hung unit. For this prototype system, Acumentrics standard fuel cell control board was utilized and is mounted on the side of the unit. Commercially available relays and flame safeguard systems were utilized to integrate with the peak burner system. For a commercial unit, this control board would be custom designed and integrated into the overall package.

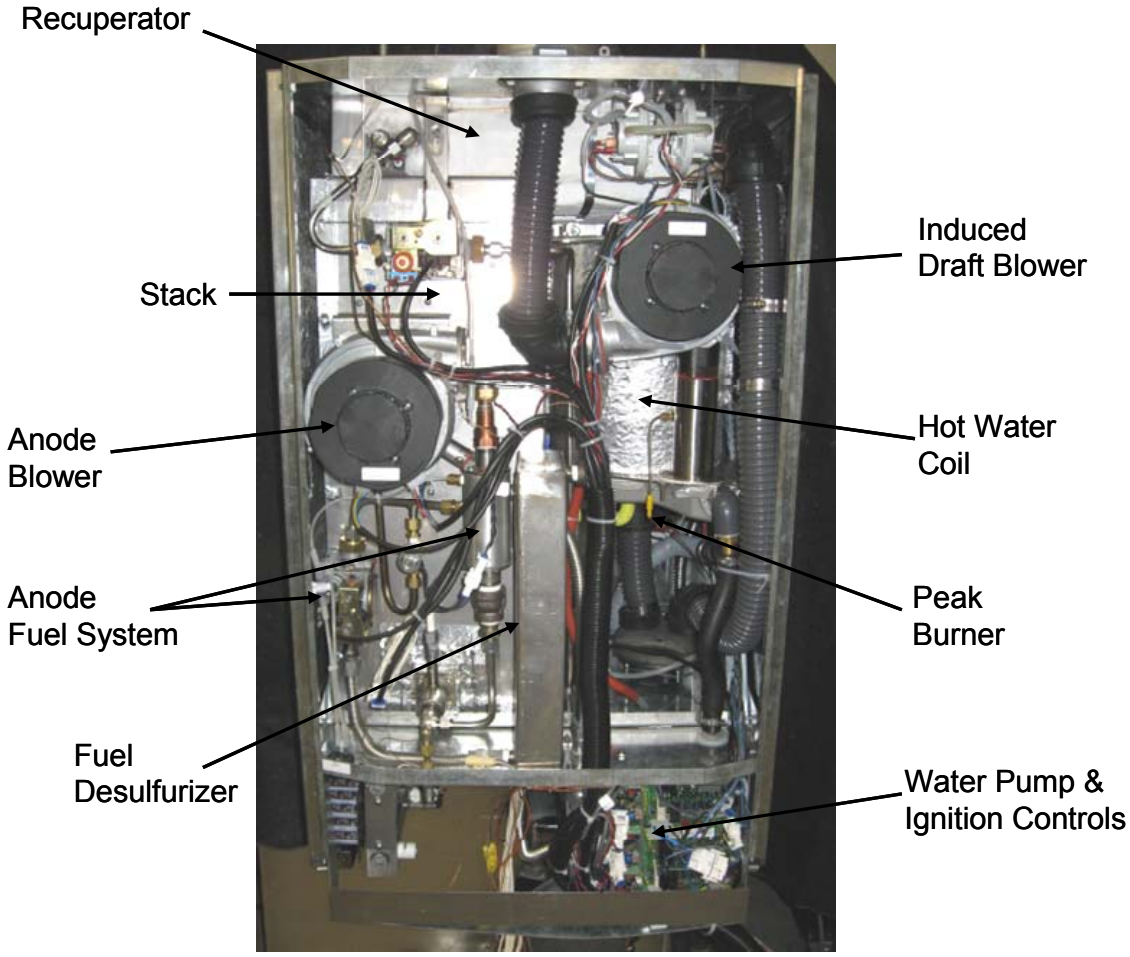

Figure 2 Combined Heat and Power System (front view)

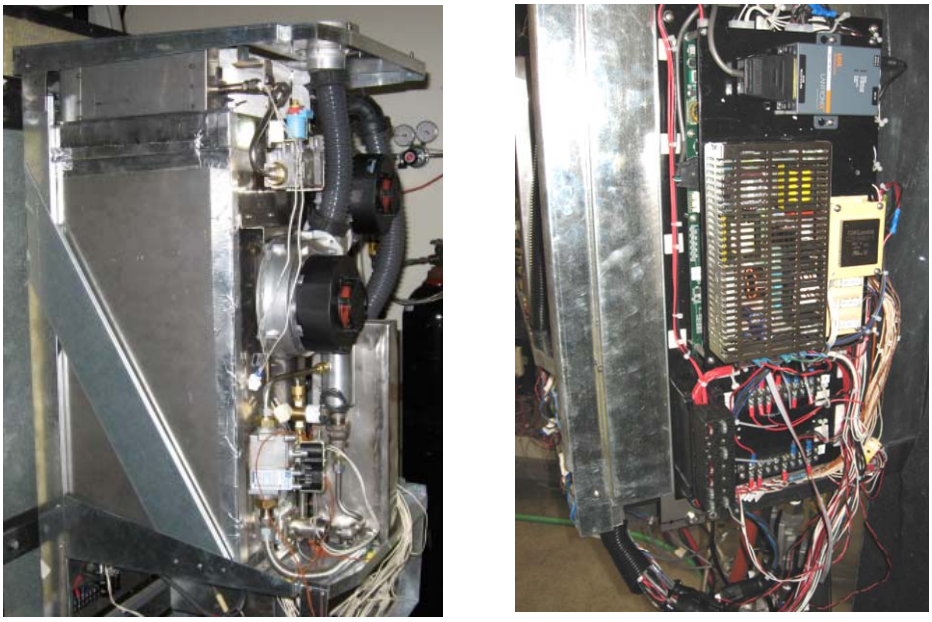

Figure 3 Combined Heat and Power System (side views)

Another 28 cell stack was designed, built and tested for inclusion into the integrated Combined Heat and Power System. As with the previous stack, 22 mm diameter triple chromite cells were utilized with all cells connected in series in a 4 by 7 array. The cells were connected to the cell caps via cement.

The stack was reduced and conditioned in Stack Tester #1. No load, reducing conditions were held for 20 hours followed by a 25 hour conditioning period. At the end of the conditioning a v-j curve was obtained (Figure 4).

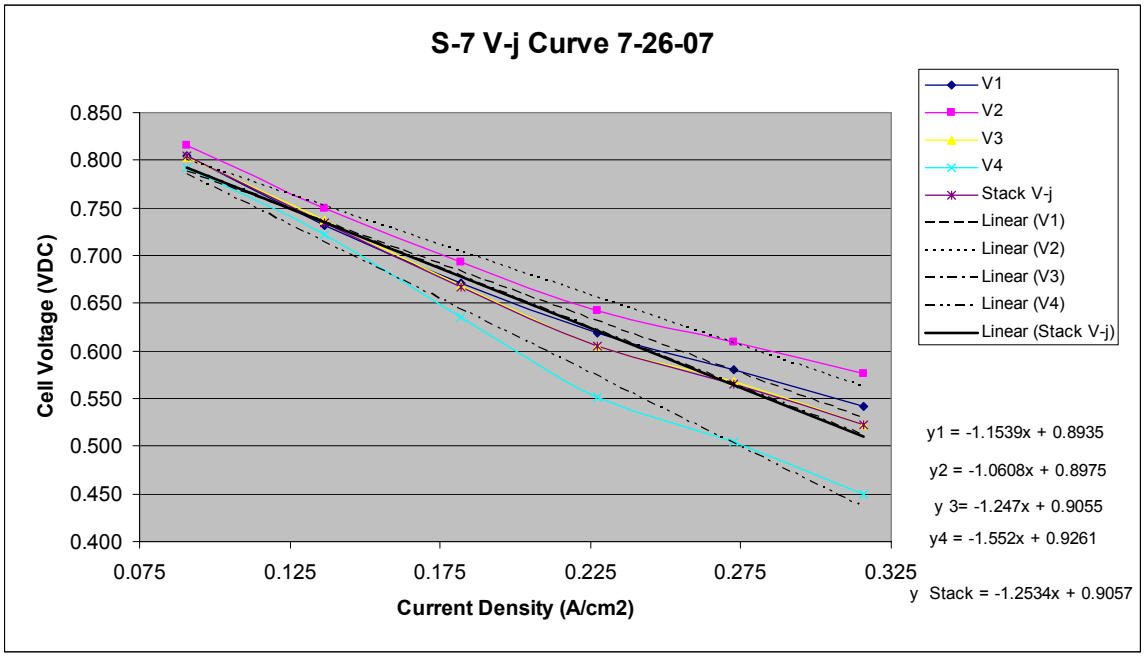

Figure 4 Initial v-j Curve S-7

Upon removal from the stack tester, a cracked cell was detected on the outboard side of layer 3 just above the first chromite band. As shown in Figure 5, there was melting of the cathode collection wires in this vicinity including on the adjacent cell on layer 2. Both cells were replaced and the stack again reduced and conditioned in Stack Tester #1. The subsequent v-j curve is shown in Figure 6. There was a considerable drop off in performance in layer 4 after the repair and thermal cycle. This layer has consistently underperformed the other layers during the stack test and this phenomenon is subject of detailed investigation. This layer which is the first to see the incoming cathode air is subject to the greatest temperature transients as well as temperature gradients which may be causing the poor performance.

Figure 5 Cracked Cell After Initial Conditioning

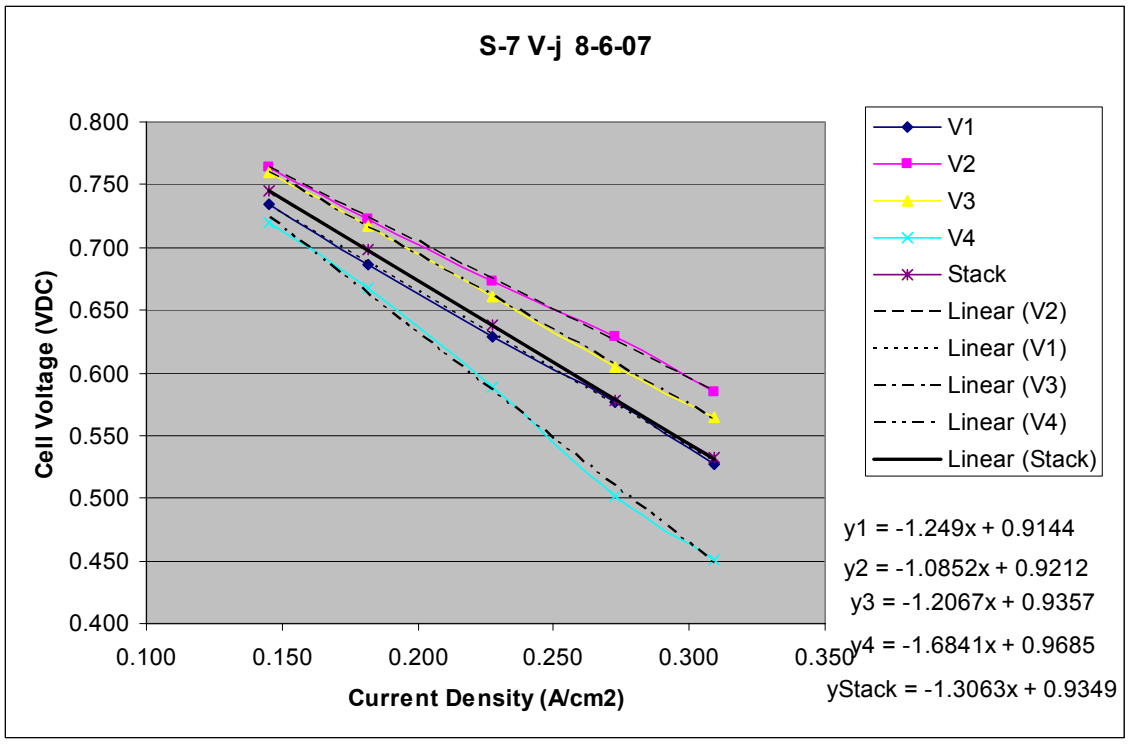

Figure 6 V-j Curve After Cell Replacement

The stack was then incorporated into an axial flow hot box for integration into the Combined Heat and Power System. The hot box was similar to that previously described for Stack 5 with the notable change that bottom penetrations for the power, voltage sense and thermocouple wires were changed to side penetrations to accommodate easier installation and removal of the hot box into the integrated system frame. Voltage and temperature lifecharts for the main 10 day test period are shown in Figure 7& Figure 8.

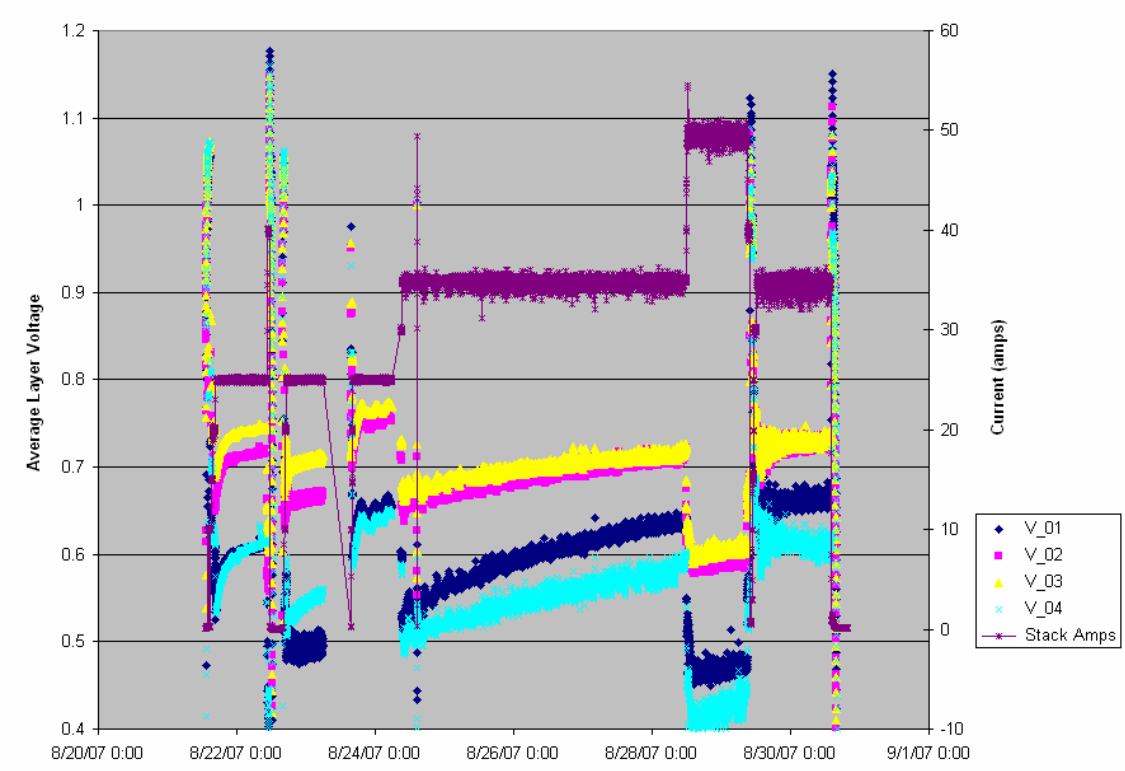

Figure 7 Layer Voltage and Current vs Time

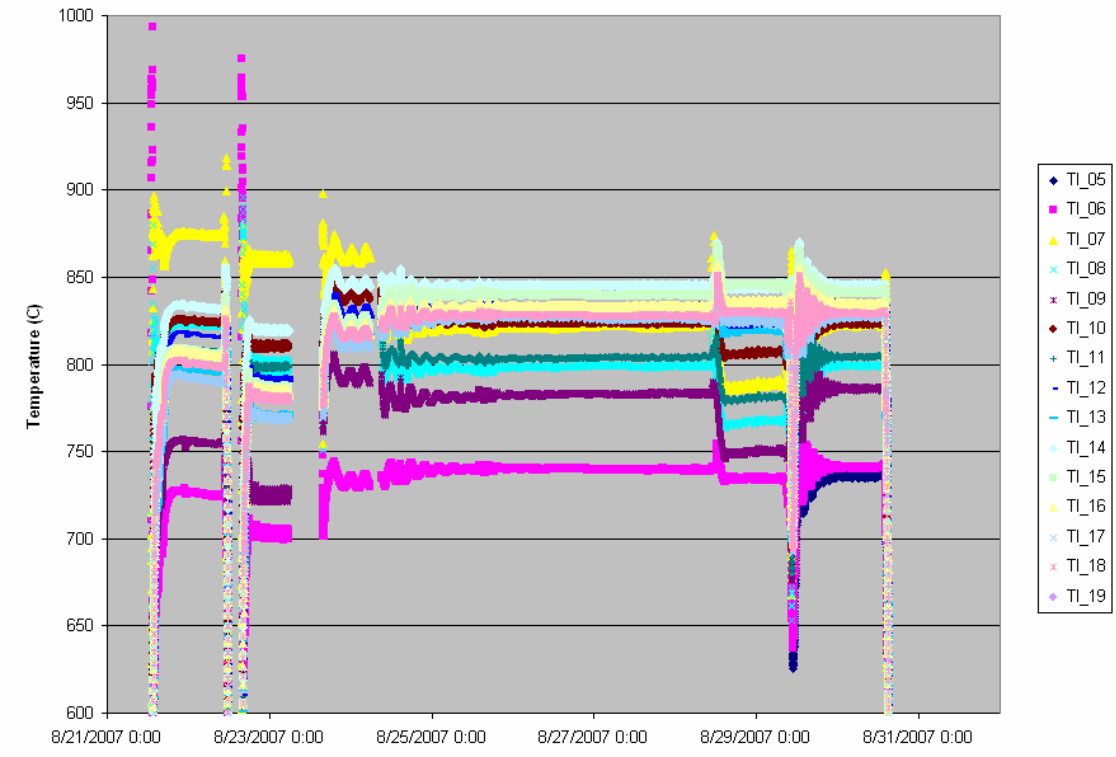

Figure 8 Stack Temperatures vs Time

During the test, a set of v-j curves were obtained (Figure 9). Unlike the earlier stack tester v-j's where the fuel utilization and temperatures were held nearly constant, the fuel utilization was varied to maintain system temperatures and even with this variation there is some change in the cell temperature as the power is varied. Also shown in Figure 10 is a typical stack temperature distribution where B, M, T correspond to thermocouples just above the bottom, middle and top chromite interconnect bands at the relative position shown.

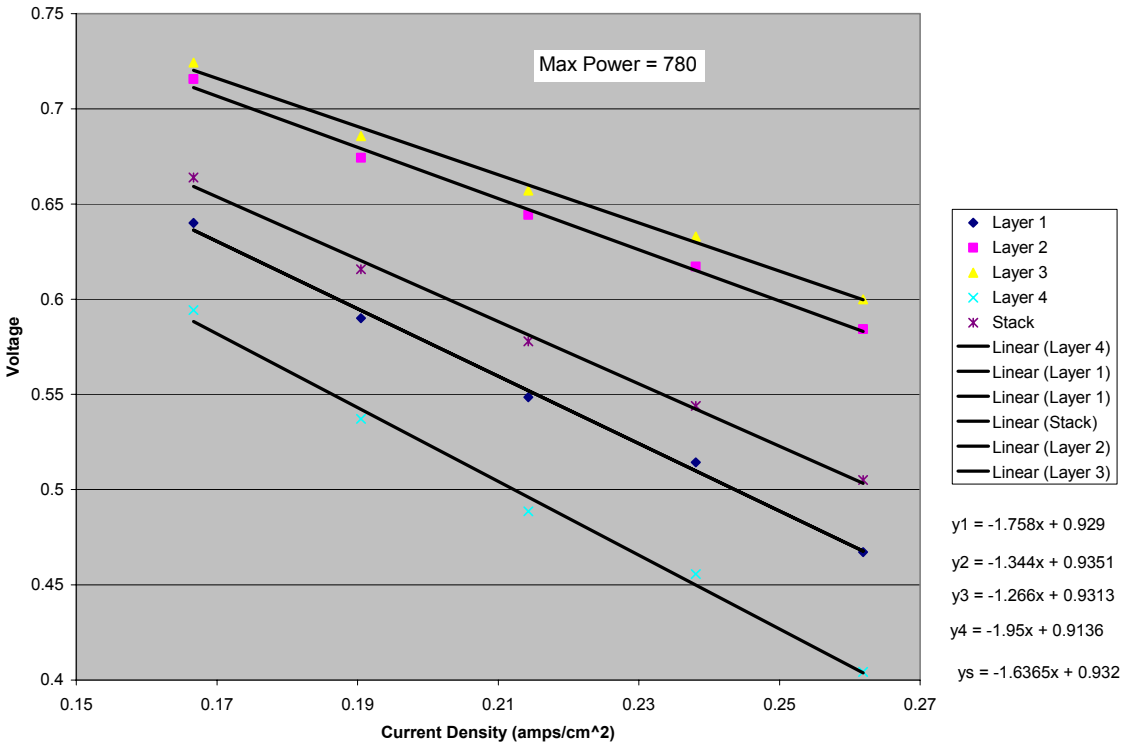

Figure 9 Integrated Test V-j Curves

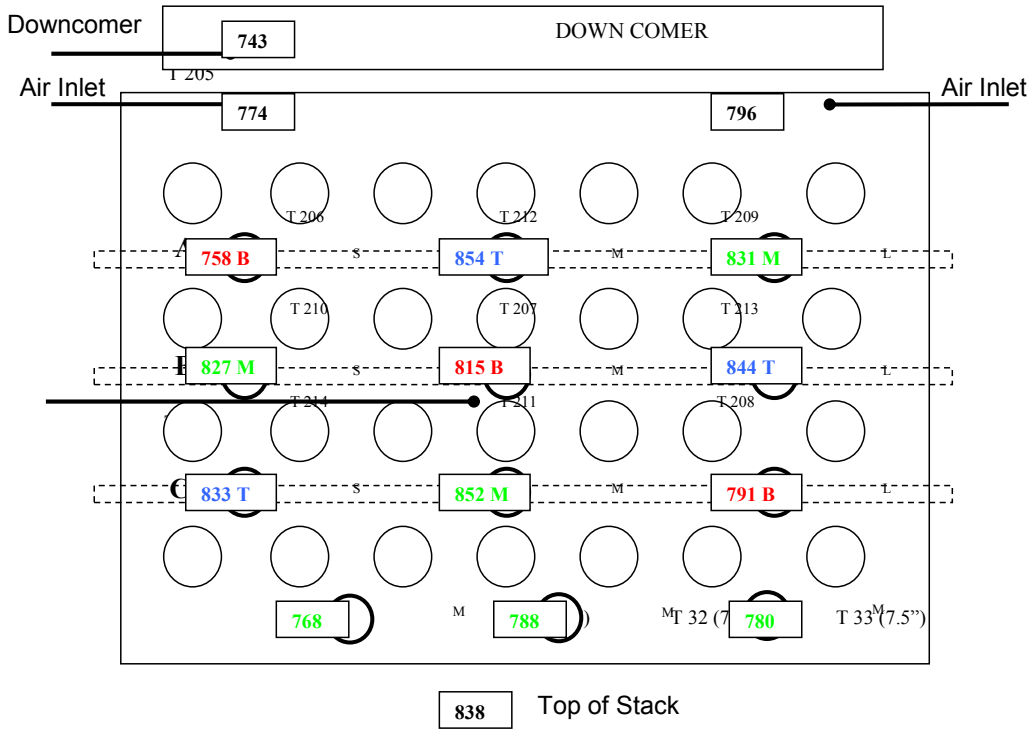

Figure 10 Stack Temperature Distribution

Stack Temperature Distribution – 50 amps, 75% Fuel Utilization

Under the operating conditions noted above the thermal performance of the system is depicted in Figure 11. The thermal recovery to the hot water system is 1 to 2 kW and the exhaust leaving the coil is only two degrees or so above the incoming water temperature. At 625 watts electrical power, the DC electrical efficiency on a Lower Heating Value (LHV) basis is approximately 30% and the overall efficiency is 80-90%. The scatter in the thermal output data and the range given for the overall efficiency is a result of the inaccuracy in measuring the hot water coil inlet and outlet temperatures. K type thermocouples were utilized and at the relative low water temperatures there was a relatively large amount of noise in the temperature measurements. These thermocouples will need to be replaced with thermsisters or J type thermocouples for higher accuracy. The above results are with the peak burner off and all fuel being introduced through the fuel cell.

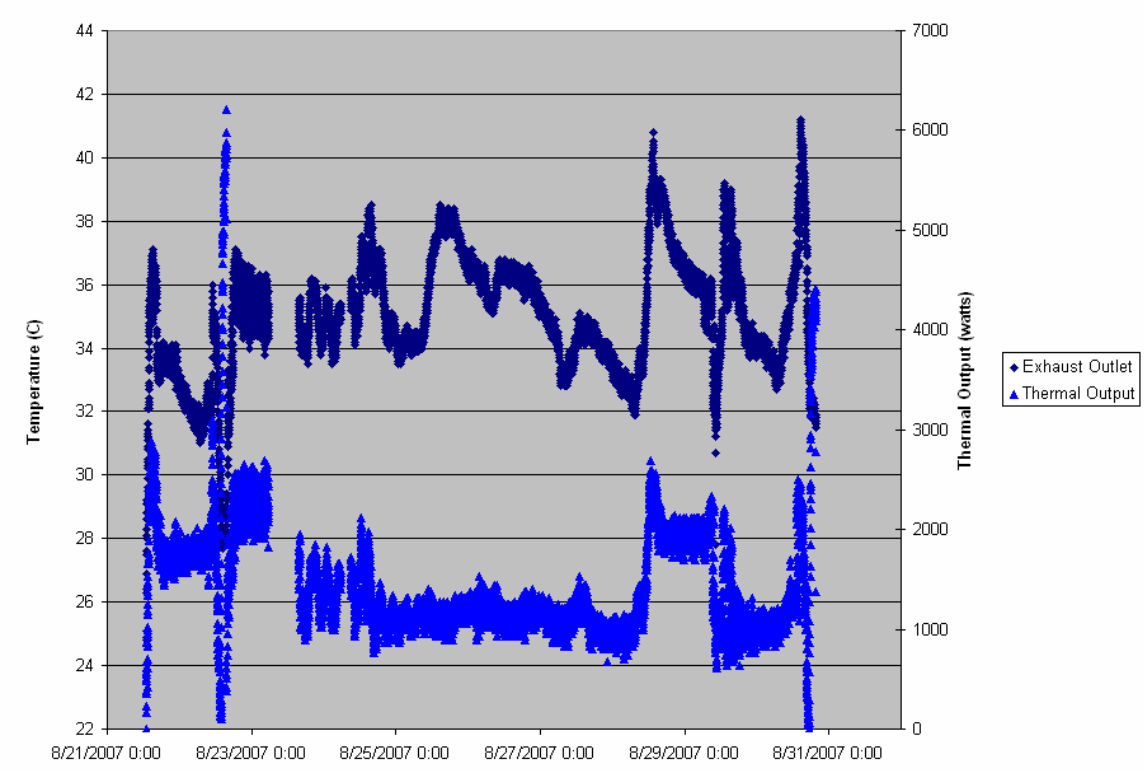

Figure 11 System Thermal Output (Fuel Cell Only)

Task 3: Proof of concept-afterburner.

During the preceding quarter, work has focused upon further developing plasma sprayed interconnects to allow multiple current take-off points on isopressed tubes. The use of these multiple current take-off points shortens the cell current path and therefore results in higher performance cells which are more efficient in their use of fuel. This in turn aligns the project further with the president's goal of reducing dependence on foreign oil and gas. Work has also been progressing well into evaluating the feasibility of isopressed closed one end base tubes with a view to eliminating the currently used brazing methodology of sealing. This will again result in increased efficiency cells through enhancing the gas tight nature of the tube and in turn maximize CO_2 sequestration. A discussion of the work carried out in each of the previously outlined areas is detailed below.

Plasma Sprayed Interconnects (IC)

Trials to develop a plasma sprayed interconnect have been successful in that working cells have been produced with multiple bands on each tube. This has resulted in a significant improvement in the performance of the cell. The main focus of the work carried out over the last quarter has been concerned with optimization of this applied interconnect.

Early interconnect development work resulted in the requirement of a two layer spraying process, consisting of an initial layer or bond coat over which is applied the chromite or top coat layer. Initial trials determined that spraying of the chromite top coat without the bond coat resulted in delamination of this layer from the cell.

It is considered that the presence of the bond coat could hinder the performance of cells and therefore efficiency due to increased current path length and localized oxidation at the anode interconnect interface. In addition, the bond coat produces a different spray pattern to the chromite top coat, causing alignment issues when trying to coat over with lanthanum chromite. This in turn leads to interconnect bands that are wider than required, thus reducing the cell active area. To try to improve cell performance and therefore efficiency, spray tests were carried out in an attempt to eliminate the necessity of the bond coat during plasma spraying. The experimental work to effect this change is detailed below.

The lanthanum chromite top coat was dried at 100^{o}C before loading the powder feed hopper of the plasma spray unit. The recently developed robotic plasma spray system was then used to fixture the tubes during spraying. This system was developed at Acumentrics and allows the spraying of eight tubes at any one time, see Figure 12. With this system, the gun moves laterally to the tubes while the tubes move up and down behind a mask which has orifice cut into it the width of the desired applied chromite band.

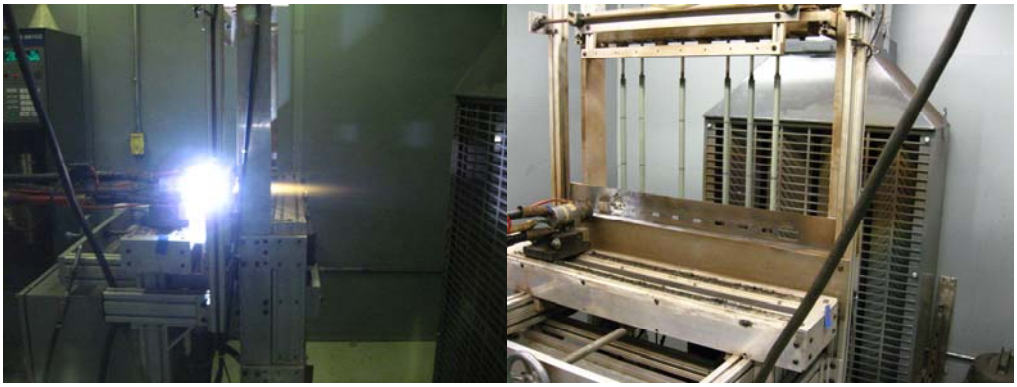

Figure 12 Plasma Fixture

Initially, experimentation was carried out using a single tube placed into the robotic fixture, followed by spraying, this methodology was used for runs 1-4 in Table 1. The production program was only utilized for run 5 where 5 tubes were coated at the same time, rather than the standard 8 tubes. Table 1 shows the coating weights for the different spray runs undertaken.

Table 1 Chromite Coating Weight and Number of Top Coats Sprayed

Run	Position	Tube #	Coating Weight (mg)	# Coats
1	8	D430172	97	12
2	8	D430146	143	18
3	8	D430195	209	24
4	8	E260216	197	24
5	1	E260222	181	24
5	3	E210263	183	24
5	5	E260099	181	24
5	7	E260285	176	24
5	8	E260110	173	24
6	8	E260214	194	21

Through optimization of gun spray parameters, namely primary and secondary gas flows, it was possible to spray only the chromite top coat and make it adhere to both the bare anode and the electrolyte overlap without the use of the conventional bond coat. Post plasma spraying, the delamination defects that are normally observed when the co-sprayed bond coat layer is not used were no longer apparent. Indeed, none of the coated tubes exhibited any defects after plasma spraying. In addition, thermal treating the sprayed cells to 1400^0C for one hour did not result in any observed delamination.

A number of the samples were then fabricated into fully working cells for performance testing while the remainders were reduced for electrical testing without a cathode coating applied. After reduction, a number of cells were selected to test the resistance between two chromite bands, with and without bond coat, during heating up to 800^oC. A 4-pt probe test was utilized. The silver leads with silver paint being applied to the surface of the chromite to limit the contact resistance (Figure 13).

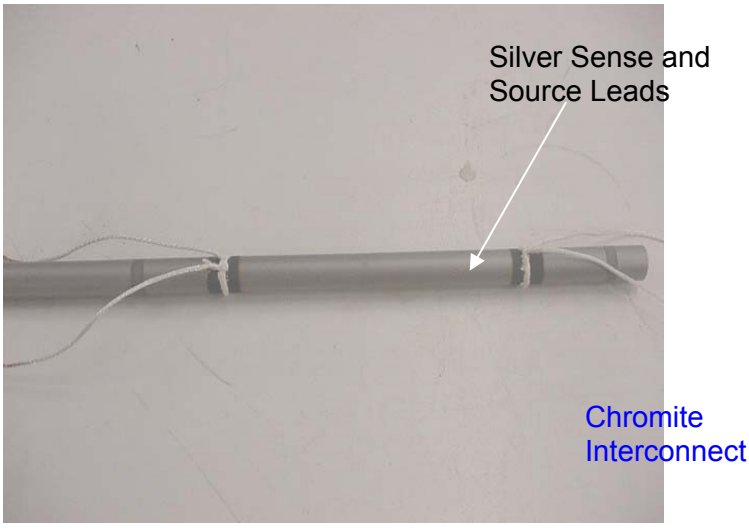

Figure 13 Point Resistance Measurement Setup Prior to Heating to 800oC

During heating nitrogen was pumped into the chamber to prevent the anode from reoxidizing. Figure 14 shows the resistance measured through the thickness of the two chromites and along the length of the reduced anode.

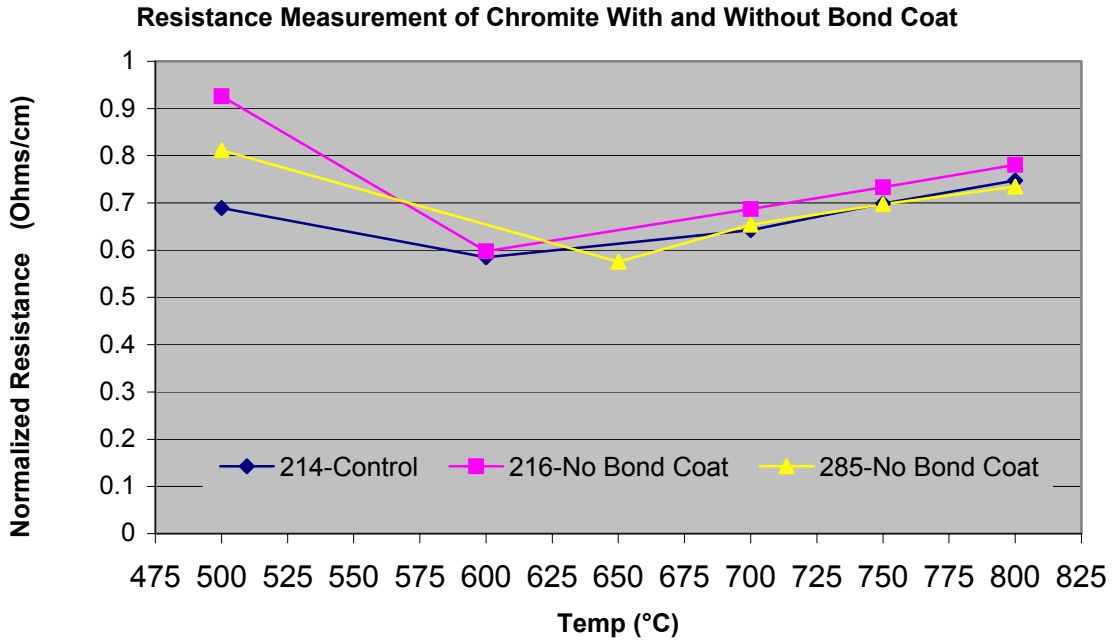

Figure 14 Resistance Measurement of Chromite With and Without Bond Coat

Figure 14 indicates through four point probe measurements, taken over a temperature range that the resistance between samples with and without bond coat does not vary significantly. However the effects of time at temperature and multiple thermal cycles have not yet been evaluated. The sprayed interconnects without bond coat still appeared intact with no noticeable delamination after one thermal cycle.

Microscopy to determine average coating thickness was then performed, see Figure 15.

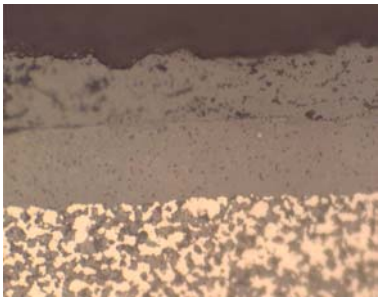

Image: Top coat layer over electrolyte. 1000x

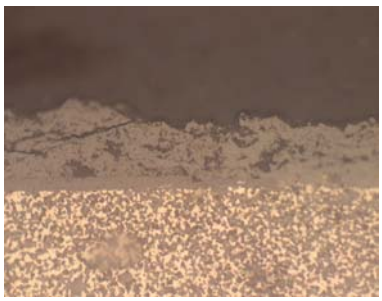

Image: Top coat layer over electrolyte and grit blast interface. 500x

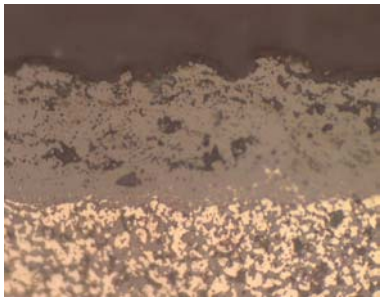

Image: Top coat layer over grit blast area. 1000x

Average	32.0	microns
Standard Deviation	7.5	microns
Relative Std. Dev.	23.4	%

Figure 15 Average Coating Thickness

In summary, cells have been successfully fabricated with plasma sprayed interconnects without the use of Acumentrics conventional bond coat. Thermal treatment of these chromite layers resulted in no observed delamination as is usually the case when bond coat is omitted from the spraying process. In addition, 4 point probe tests through two interconnects at 800˚C resulted in similar resistance measurements for standard cells and those fabricated without bond coat. Fully fabricated cells without bond coat are presently in the cell test queue waiting for performance testing. Further trials will be run to evaluate the durability of bond coat free interconnects over increasing time frames and thermal cycles.

Isostatically Pressed (IP) Closed One End (COE) Tubes

Investigations are progressing at Acumentrics into isostatically pressed closed one end tubes in an effort to improve upon the gas leak rate of the current braze cap solution and produce cells with higher power. It is considered that with an integral ceramic closed end on the tube that gas leak from this area will be kept to an absolute minimum as no material interface exists.

It has been determined through previous firing trials that IP tubes, with a 22mm outer diameter, are required to be hang fired in order to produce a straight round tube. Acumentrics conventional horizontal firing resulted in the tubes sagging during firing producing non round tubes. The focus of recent work has been involved with optimization of the electrolyte coating methodology, through utilization of the flat plate with orifice kiln furniture detailed in the previous quarterly report.

To this end, a prototype apparatus was manufactured to demonstrate the feasibility of applying electrolyte to 22mm OD IP tubes while being supported on the new silicon carbide furniture

consisting of plates with multiple orifices. In addition to applying a vacuum to the inside of each IP tube during the electrolyte infiltration process, this equipment is also used to extract the solvent that tends to collect inside the tubes after infiltration. The solvent extraction is carried out with the IP tubes in the same orientation as dipping to simplify handling.

The apparatus consists of an aluminum manifold supporting stainless steel injector tubes. This manifold is positioned on top of the IP tubes after they are loaded onto the new SiC furniture. A soft foam rubber gasket bonded to the lower surface of the manifold provides a seal between the end faces of the IP tubes and the manifold. The gasket material selected was chosen to enable sealing to be achieved with minimal pressure to the tube end faces.

The stainless steel injector tubes reach deep inside each IP tube to within approximately 12 mm from the bottom faces. A short length of loose fitting silicone tubing is attached to the end of each injector and these are positioned so that their ends contact the bottom inside surface of the IP tubes. A small notch is cut into the ends of the silicone tubing to prevent “blinding”. The aluminum manifold also incorporates ports positioned close to the injector tubes that are plumbed to a three way valve connected to atmosphere, see Figure 16 & Figure 17.

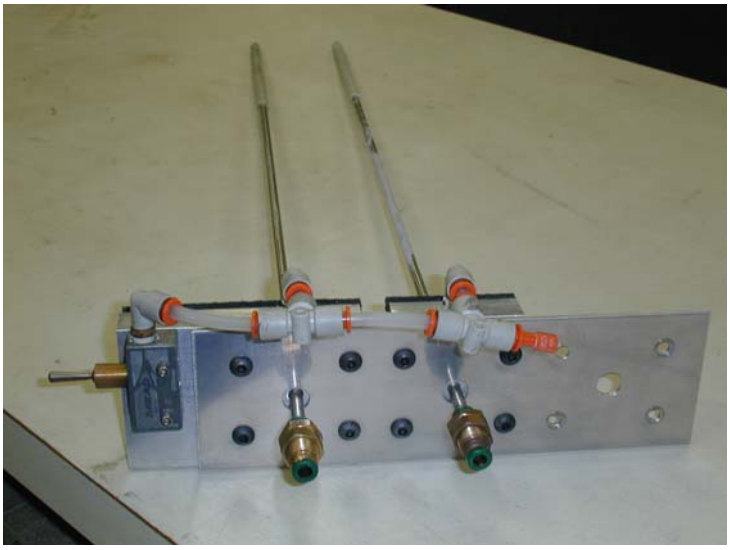

Figure 16 Manifold

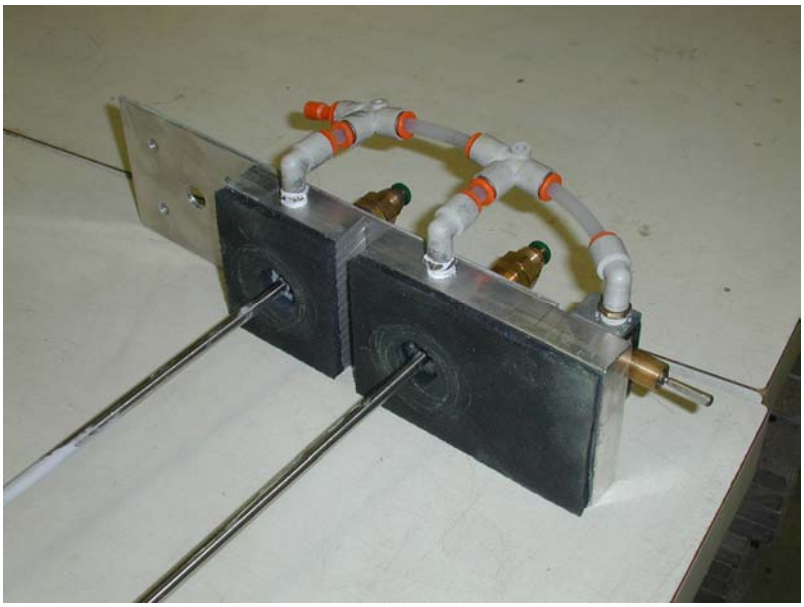

Figure 17 Pictures of prototype apparatus used in trials

Operation of the dipping apparatus is simple and involves placement on top of the IP tubes which are pre-positioned in the recently developed silicon carbide furniture before a vacuum is applied to the injector tubes via individual pumps. When a pre-determined vacuum level is reached, the IP tubes are lowered into a tank of electrolyte slurry for a set amount of time. The tubes are then raised quickly out of the slurry with excess electrolyte draining off back into the tank.
A three way valve is then actuated to gradually increase the pressure inside the tubes. This has the effect of assisting the vacuum pump to remove the solvent remaining at the bottom of each tube. The solvent is collected in traps connected between the vacuum pumps and injector tubes. Figure 17, Figure 18, Figure 19, & Figure 20 show the prototype dipping apparatus being used.

Figure 18 IP tubes shown hanging in new silicon carbide furniture

Figure 19 Apparatus positioned on top of IP tubes with vacuum applied

Figure 20 IP tubes immersed in electrolyte

Figure 21 IP tubes after electrolyte dipping

After electrolyte dipping, the tubes are then electrolyte fired to produce a dense leak tight electrolyte layer. An evaluation of the first pressed 22mm OD tubes to go on cell testing revealed that these cells were susceptible to changes in fuel utilization, suggesting that the cells leak in some fashion. An experiment was therefore conducted to investigate the electrolyte and plasma sprayed chromite-band region of the cell to determine coating uniformity, thickness, and porosity, with a view to eliminating leak. Table 2 shows microscopy details concerning electrolyte and chromite thickness from a number of sample cells.

Table 2 Microscopy Details

	Electrolyte	**Chromite**
AVG (μm)	22.57	39.35
STDV	3.42	15.99
REL STDV	15.14%	40.63%

The electrolyte coating thickness average of 22.57 μm is similar to standard production cells with a standard deviation of 3.42 μm or 15.14%. The chromite spray coating thickness is also similar to standard production cells, but the coating was not uniform throughout as is the case for production cells. The standard deviation of measured chromite thickness was 15 μm or 40 %. The thickness of the electrolyte and chromite coatings therefore does not appear to be the reason for fuel loss during testing of these new anode cells. Further micro investigation however revealed porosity in the electrolyte microstructure, see Figure 22.

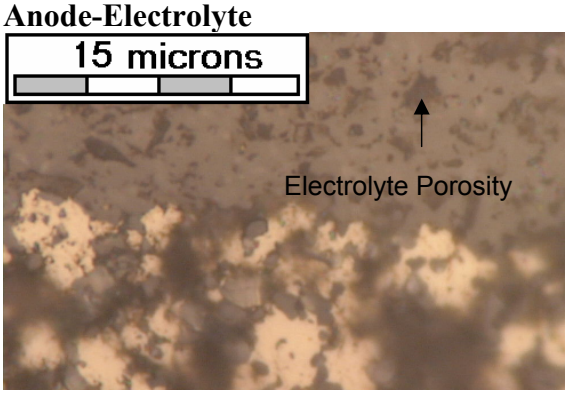

Anode-Electrolyte Phase Boundary:
(Isopressed Tube)

This image is from the reduced sample at a magnification of 1500X. Notice a relatively large number of darkish voids in the area of the electrolyte.

Figure 22 Electrolyte Porosity

No porosity was observed in the chromite layer, however significant porosity in the form of dark voids were observed in the electrolyte layer which were subsequently measured for size. Most of the voids consisted of small pores in the range of 1-3 μm although some voids were found in the electrolyte that measured up to 5 μm in diameter. In order to estimate the severity of porosity found in the electrolyte, micrographs of a previously determined porous electrolyte which had been cell tested and found to have poor performance were located and used for comparison, the detail of which is explained below.

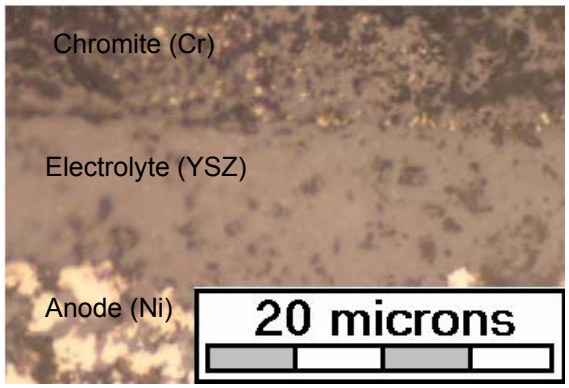

Anode-Electrolyte-Chromite (Isopressed Tube):

This is the same IP tube sample as above but taken in a different area of the tube at 1000X magnification.

BF_1000X, Reduced

Figure 23 Anode-Electrolyte-Chromite

Figure 23 is a section from the same 22mm OD sample discussed above but is at 1000x magnification and can be compared to the micrograph of a previously determined porous electrolyte phase material, see Figure 24. Both images show severe comparable porosity.

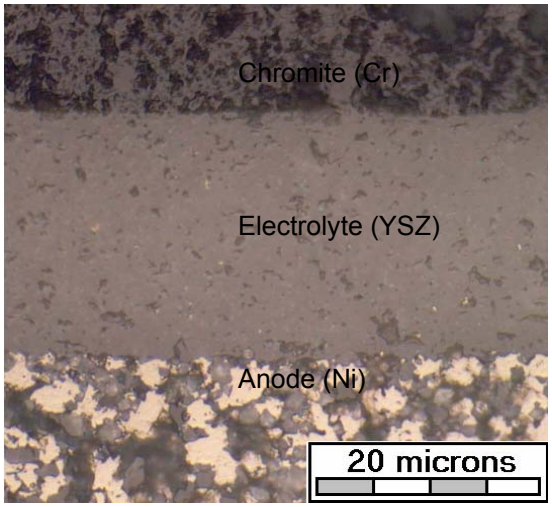

Figure 24 Anode-Electrolyte-Chromite

A poorly sintered electrolyte coating on the IP tube left porosity in the electrolyte phase which resulted in sensitivity to fuel concentration during testing. The thickness of the electrolyte coating and the thickness of the chromite coating were comparable with standard production cells, indicating that the level of electrolyte sintering and resultant porosity is the only factor believed to cause the issue with leakage.

To overcome this porous sintered electrolyte issue on the IP tubes, the firing parameters for both the bisque firing and the electrolyte sintering will be optimized with further testing.

Task 5: Project Management

Acumentrics Final Quarterly Report and Project Summary have been completed.

Plans for Next Quarter and Key Issues:

This is the Final Report for this contract so there are no plans for next Quarter activities.

Patents:

There are presently no patents being applied for under this award.

Publications / Presentations:

A poster presentation was made at the 2005 DOE Hydrogen Program Review in Washington, D.C. on May 24th.

A poster presentation was made at the 2006 DOE Hydrogen Program Review in Washington, D.C. on May 16th.

Task Schedule

Task Number	Project Milestones	Task Completion Date				Progress Notes
		Original Planned	Revised Planned	Actual	Percent Complete	
1	Conceptual Generator Design	9/30/04		10/09/07	100%	
2	Build Manifold Test Rigs	5/15/05		10/09/07	100%	
3	Literature Review	6/30/05		10/09/07	100%	
4	Short-Term Testing	12/1/05	9/1/06	10/09/07	100%	
5	Quarterly Reports			10/09/07	100%	

Current Budget Period: 10/01/04 to 9/30/07

Spending Schedule **Current Quarter:** 07/01/07 to 9/30/07

Budget Category	Approved Budget	Project Expenditures	
		This Quarter	Cumulative to Date
Personnel		143,241	766,021
Fringe Benefits		32,981	171,098
Travel			
Equipment			
Supplies		32,565	579,541
Contractual			
Construction			
Other			
Total Direct Charges		208,787	
Indirect Charges		83,542	1,517,447
Total		292,329	2,048,751
DOE Share	1,639,175	643,613	2,048,751
Cost Share	409,793	58,467	409,751

Cost Share Contributions

Funding Source	Approved Cost Share		This Quarter		Cumulative to Date	
	Cash	In-Kind	Cash	In-Kind	Cash	In-Kind
Acumentrics Corp.	409,751		58,467		409,751	
Total	409,751		58,467		409,751	
Cumulative Cost Share Contributions					409,751	